AIAA SciTech Forum
8–12 January 2018, Kissimmee, Florida
2018 AIAA Aerospace Sciences Meeting

10.2514/6.2018-1771

Two-Dimensional Krypton Tagging Velocimetry (KTV-2D) Investigation of Shock-Wave/Turbulent Boundary-Layer Interaction

M. A. Mustafa* N. J. Parziale†
Stevens Institute of Technology, Hoboken, NJ 07030, USA
M. S. Smith‡ E. C. Marineau§
AEDC White Oak, Silver Spring, MD 20903, USA

Preliminary results from a two-dimensional Krypton Tagging Velocimetry (KTV-2D) investigation of a Mach 2.75 turbulent boundary and 24 degree compression corner flow are presented in this paper. KTV-2D is performed by creating a grid of tagged Kr atoms formed by intersecting laser lines and imaging the resulting fluorescence at a write step; then, after a time delay, imaging the translation of the grid by re-exciting the tagged atoms for the read step. The measurements were made in a 99% N_2 and 1% Kr gas mixture. Spatial correlation was used to extract the velocity from the data. It was found that the streamwise component of the velocity in the boundary layer agrees well with the literature; however, a consistent bias was noted in the wall-normal velocity component in the boundary-layer and compression corner flows and we provide an explanation and correction for this bias which will easily be eliminated in future experimentation (the bias was a result of procedure, not inherent in the technique). The turning angle in the compression corner flow matches the result from classical inviscid theory, bringing confidence to the results.

Nomenclature

$\dot{m}$ = Mass flow rate, ($\mathrm{kgm^{-1}s^{-1}}$)
A = Area, ($\mathrm{m^2}$)
C = Discharge coefficient, (-)
P = Pressure, (Pa)
ρ = Density, ($\mathrm{kgm^{-3}}$)
γ = Ratio of specific heats, (-)
Ma = Mach number, (-)
T = Temperature, (-)
r = Recovery Factor, (-)
Pr = Prandlt number, (-)
u = Streamwise velocity component, ($\mathrm{ms^{-1}}$)
v = Normal velocity component, ($\mathrm{ms^{-1}}$)
u' = Fluctuating streamwise velocity component, ($\mathrm{ms^{-1}}$)
v' = Fluctuating normal velocity component, ($\mathrm{ms^{-1}}$)
δ = Boundary layer thickness, (m)
u_τ = Friction velocity, ($\mathrm{ms^{-1}}$)
Θ = Momentum thickness, (-)
K = Correlation coefficient, (-)

*Graduate Student, Mechanical Engineering, Castle Point on Hudson, Hoboken, New Jersey, 07030.
†Assistant Professor, Mechanical Engineering, Castle Point on Hudson, Hoboken, New Jersey, 07030, AIAA Member.
‡Senior Research Engineer, National Aerospace Solutions, Silver Spring, MD 20903, Senior AIAA Member
§Chief Technologist, AEDC White Oak, Silver Spring, MD 20903, Senior AIAA Member.

I = Intensity image, (-)
σ = Standard Deviation, (-)
R = Specific gas constant, ($JKg^{-1}K^{-1}$)

Subscript
$mean$ = Average value
∞ = Free stream
w = Wall
Θ = Based on momentum thickness
rms = Root mean squared
1 = Write image
2 = Read image

I. Introduction

Turbulence and shock waves are ubiquitous in high-speed flight, which leads to significant challenges in understanding compressible flow over flight vehicles. On its own, understanding the turbulent nature of compressible flow is a daunting task; the presence of shock waves alters/adds time and length scales which further complicate matters. Two characteristics of shock-wave/turbulent boundary-layer interaction are: 1) the unsteady flow field associated with separation;[1] and, 2) turbulence amplification across shocks by way of increase in velocity fluctuations.[2] A change in the velocity-fluctuation amplitude changes the shear stresses, heat transfer rates and mixing properties of the flow. All these quantities have design implications; consequently, to accurately predict the aerothermodynamic loads on supersonic/hypersonic vehicles, it is necessary to understand shock-wave/turbulent boundary-layer interactions.

To this end, it is necessary to develop experimental techniques to make measurements in high-speed flows. Two ubiquitous techniques are Laser Doppler Velocimetry (LDV) and Particle Image Velocimetry (PIV).[3] These particle-based measurements rely on the assumption that the tracer particles travel identically with the flow. However, the particle response time can be inadequate in low-density flows with short time scales. Loth[4] found that at low densities the Knudsen number of a particle can become large. This represents a fundamental limitation of particle-based techniques because the slip condition at the particle surface culminates in reduced response time. Several researchers[5–7] have examined the response of particles to shock waves in an effort to quantify particle response time. Williams et al.[8] suggest that "particle frequency response analyses based solely on shock response tests may well have overestimated the response to turbulence."

Measurement of velocity fluctuations in high-speed turbulent boundary layers is an example that brings the particle-response time limitation to bear. Lowe et al.[9] asserts that "[s]trong evidence exists that experimental data gathered in high speed flows using particle-based techniques exhibit significant particle lag effects on magnitudes of turbulence quantities." This assertion was based on an experimental LDV campaign in a Mach 2.0 turbulent boundary layer, and the authors made particle-lag corrections to address discrepancies in their data. Recent work by Brooks et al.[10] found that particle-lag effects are more pronounced in the turbulence quantities associated with the wall-normal velocity than the streamwise velocity. This is because the wall-normal velocity fluctuation spectrum is flatter (has more high-frequency content) than its streamwise counterpart.

An attractive alternative to particle-based techniques is tagging velocimetry. Tagging velocimetry[11] is typically performed in gases by tracking the fluorescence of a native, seeded, or synthesized gas. Its advantage over PIV techniques in high-speed facilities is that it is not limited by timing issues associated with tracer injection[12] or reduced particle response at Knudsen and Reynolds numbers[4] characteristic of high-speed wind tunnels. Methods of tagging velocimetry include the VENOM,[13–17] APART,[18–20] RELIEF,[21–25] FLEET,[26,27] STARFLEET,[28] PLEET,[29] argon,[30] iodine,[31,32] sodium,[33] acetone,[34–36] NH[37] and the hydroxyl group techniques,[38–40] among others.[41–45]

In this work, we use Krypton Tagging Velocimetry (KTV). KTV was first demonstrated by Parziale et al.[46,47] to measure the velocity along the centerline of an underexpanded jet of N_2/Kr mixtures. Following that work, Zahradka et al.[48,49] used KTV to make measurements of the mean and fluctuating turbulent boundary-layer profiles in a Mach 2.7 flow. Mustafa et al.[50] used KTV to measure seven simultaneous profiles

of streamwise velocity and velocity fluctuations in the incoming boundary layer and immediately upstream of a 24-degree compression corner in a $M_\infty = 2.8$, $\mathrm{Re}_\Theta = 1750$, 99% N_2/1% Kr shock-wave/turbulent boundary-layer interaction. Recently, KTV was implemented in the Stevens Institute of Technology Shock Tube by Mustafa et al.[51] to measure the freestream velocity behind a Mach 3 shock. In addition, KTV has been demonstrated to work in the freestream of the large-scale AEDC Hypervelocity Tunnel 9.[52]

To date, KTV has resulted in one-dimensional velocimetry measurements. In this paper, we present a preliminary two-dimensional Krypton Tagging Velocimetry (KTV-2D) investigation of a Mach 2.75 turbulent boundary and 24 degree compression corner flow. Details on the velocimetry technique and facility are given along with the data reduction algorithm.

II. Facility and Experimental Setup

The experiments were performed in the AEDC Mach 3 Calibration Tunnel (M3CT) in Silver Spring, MD (Fig. 1. The tunnel is comprised of a large vacuum tank attached to a converging diverging nozzle. A flexible isolation bag was added upstream of the orifice to contain the 99% N_2/1% Kr gas mixture. The flexibility ensured that the mixture stayed at constant ambient pressure. Fig. 2 shows the experimental setup with the modifications. A valve is cycled downstream of the nozzle to run the tunnel. The run condition calculations can be found in Zahradka et al.[49] and Mustafa et al.[50] Conditions are listed in Table 1.

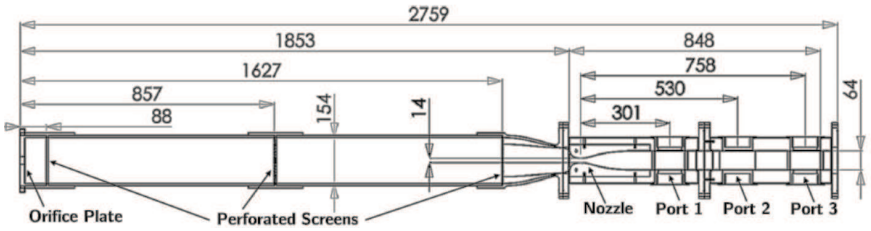

Figure 1: Sketch of AEDC Mach 3 Calibration Tunnel (M3CT). Dimensions in millimeters. The measurements are made at "Port 2."

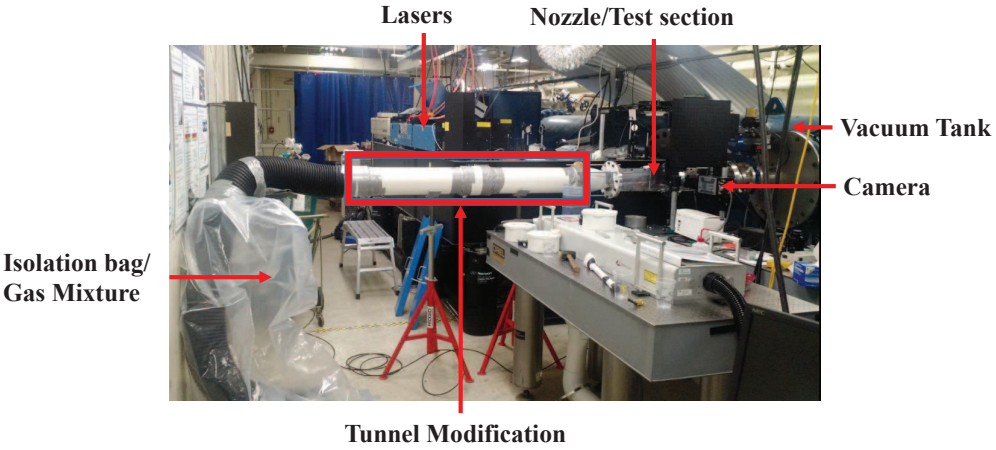

Figure 2: Experimental setup.

Table 1: M_∞, P_∞, T_∞, ρ_∞, $\mathrm{Re}_\infty^{unit}$, Re_Θ, and U_∞ are the Mach number, pressure, temperature, density, unit Reynolds number, momentum-thickness Reynolds number, and velocity for each experiment. τ_m and x_m are the calculated time and distance scale, respectively, for the decay of the metastable Kr state.

Experiment	M_∞ (-)	P_∞ (Pa)	T_∞ (K)	ρ_∞ (kg/m^3)	$\mathrm{Re}_\infty^{unit}$ (1/m)	Re_Θ (-)	U_∞ (mm/µs)	$10\tau_m$ (µs)	x_m (mm)
M3 AEDC - 19.1 mm OP	2.77	1010	118	0.030	2.30e6	1750	0.612	4.1	2.5

A mean Schlieren image of 100 frames of the flow over the 24 degree wedge is presented as Fig. 3. The mean shock position was found using local fits of the image intensity; the shock angle was determined to be ≈ 32 degrees, consistent with previous KTV work.[50]

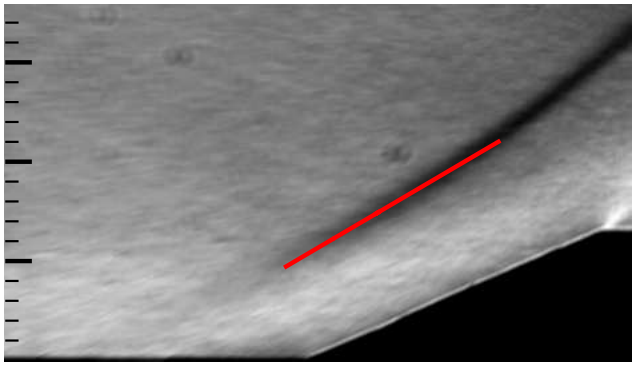

Figure 3: Schlieren of 24 degree wedge with 0.019 m orifice plate. Flow is left to right. Major tick marks are 10 mm. Mean shock position shown in red.

III. Krypton Tagging Velocimetry (KTV)

In this paper, Krypton Tagging Velocimetry (KTV) was used to make measurements in a Mach 2.75 boundary layer and compression corner flow. Relative to other tagging velocimetry techniques, KTV relies on a chemically inert tracer, which may enable it to broaden the applicability of tagging velocimetry because it can be applied in gas flows where the chemical composition is difficult to prescribe or predict. The use of a metastable noble gas as a tagging velocimetry tracer was first suggested by Mills et al.[53] and Balla and Everheart.[54]

This work utilized the excitation scheme used by Mustafa et al.[50] which when compared to the excitation scheme used in previous KTV work,[46–49] results in approximately twice as much fluorescence.[51] Using this excitation scheme KTV is performed in the following steps according to the energy level diagram shown in Fig. 4.

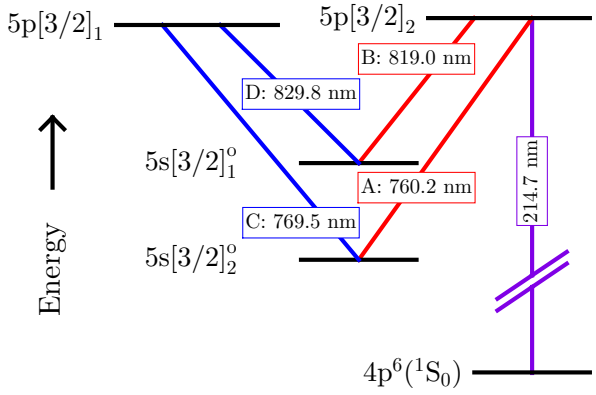

Figure 4: Energy diagram for excitation scheme. Racah nl[K]J notation, A, B, C and D represent the transitions between the states.

1. Seed a base flow with krypton globally.
2. Photosynthesize metastable krypton atoms with a pulsed tunable laser to form the tagged tracer: two-photon excitation of $4p^6(^1S_0) \rightarrow 5p[3/2]_2$ (214.7 nm) and rapid decay to resonance state $5p[3/2]_2 \rightarrow 5s[3/2]^o_1$ (819.0 nm, transition B) and metastable state $5p[3/2]_2 \rightarrow 5s[3/2]^o_2$ (760.2 nm, transition A). We estimate that the creation of the metastable atoms which comprise the "write line" takes approximately 50 ns.[55] The position of the write line is marked by the fluorescence from the $5p[3/2]_2 \rightarrow 5s[3/2]^o_1$ transitions (819.0 nm, transition B), and is recorded with a camera positioned normal to the flow.
3. Record the displacement of the tagged metastable krypton by imaging the laser induced fluorescence (LIF) that is produced with an additional pulsed tunable laser: excite $5p[3/2]_1$ level by $5s[3/2]^o_2 \rightarrow 5p[3/2]_1$ transition with laser sheet (769.5 nm, transition C) and read spontaneous emission of $5p[3/2]_1 \rightarrow 5s[3/2]^o_1$ (829.8 nm, transition D) transitions with a camera positioned normal to the flow.

The experiment was run using two tunable lasers to provide the 214.7 nm (write) and 769.5 nm (read) laser beams required for KTV (schematic in Fig. 5). The write laser consisted of a frequency doubled Quanta Ray Pro-350 Nd:YAG laser and a frequency tripled Sirah PrecisionScan Dye Laser. The Nd:YAG laser pumped the dye laser with 1000 mJ/pulse at a wavelength of 532 nm. The dye in the laser was DCM with a dimethyl sulfoxide (DMSO) solvent, and the laser was tuned to output a 644.1 nm beam. Frequency tripling of the dye-laser output was performed using Sirah tripling optics (THU 205).

The write-laser beam setup can result in approximately 10-13 mJ/pulse; however, approximately 7 mJ was used for this experiment by reducing the Nd:YAG pump-laser power. The wavelength was 214.7 nm, with a linewidth of approximately 0.045 cm^{-1}, a pulsewidth of approximately 7 ns, and a repetition rate of 10 Hz. The write-laser beam was split into two beams with a beam splitter designed for use with a 193 nm Excimer laser (Lambda Research XPR-SWI-4002U-50R-193-45U). To evenly split the laser beams the beam-splitter mount was rotated slightly about the vertical axis. The two beams were directed into the test section with 1 inch 5th-harmonic Nd:YAG laser mirrors (IDEX Y5-1025-45) and focused to several narrow waists in the test section with a $f = 100$ mm fused-silica microlens array (SUSS MicroOptics Nr. 18-00127) to form the lines in the streamwise direction and a $f = 100$ mm fused-silica cylindrical lens to focus the lines in the spanwise direction. Neglecting losses from the mirrors, lenses, and windows, we estimate that the energy per write line is approximately 300 µJ/pulse.

The read laser consisted of a frequency doubled Quanta Ray Pro-350 Nd:YAG laser and a Sirah PrecisionScan Dye Laser. The Nd:YAG laser pumped the dye laser with 215 mJ/pulse at a wavelength of 532 nm. The dye in the laser was Styryl 8 with a DMSO solvent, and the laser was tuned to output a 769.5 nm beam.

The read-laser beam setup resulted in approximately 5 mJ/pulse, with a wavelength of 769.5 nm, a linewidth of approximately 0.025 cm^{-1}, a pulsewidth of approximately 7 ns, and a repetition rate of 10 Hz. The read-laser beam was directed into the test section using 2 inch broadband dielectric mirrors (Thorlabs BB2-E02), and expanded to a beam of ≈ 40 mm diameter with a $f = -400$ mm fused silica cylindrical lens. This "read beam" re-excites the metastable Kr tracer atoms so that their displacement can be measured.

The laser and camera timing are controlled by a pulse-delay generator (SRS DG645). The intensified camera used for all experiments is a 16-bit Princeton Instruments PIMAX-4 1024x1024 with an 18-mm grade 1, Gen III extended red filmless intensifier w/ P46 phosphor (PM4-1024i-HR-FG-18-P46-CM). The lens used is a Nikon NIKKOR 24-85mm f/2.8-4D in "macro" mode and positioned approximately 200 mm from the write/read location. Two high-precision 800 nm longpass filters (Thorlabs FELH0800, transmission of 3.5e-4% at the read-laser wavelength of 769.5 nm) are placed in series between the lens and the intensifier to minimize the noise resulting from the read-laser pulse reflection and scatter from solid surfaces. The gain is set to 100% with no pixel binning and only recording the read images to ensure a 10 Hz frame rate. A set of write images were recorded with the tunnel off prior to each run. The camera gate was opened for 50 ns immediately following the read-laser pulse to capture the spontaneous emission of $5p[3/2]_1 \rightarrow 5s[3/2]^o_1$ (829.8 nm) transitions.

The beams enter the test section in the same plane and intersect at ≈ 140 degrees. The locations of the intersections were adjustable and so for the boundary layers experiments, three sets were done with the intersections sequentially moved further from the wall in order to get data at more points. In the case of the wedge, three sets were also done but this time the position of the wedge was varied to get data before and

after the shock. In each set, roughly 600 frames were collected.

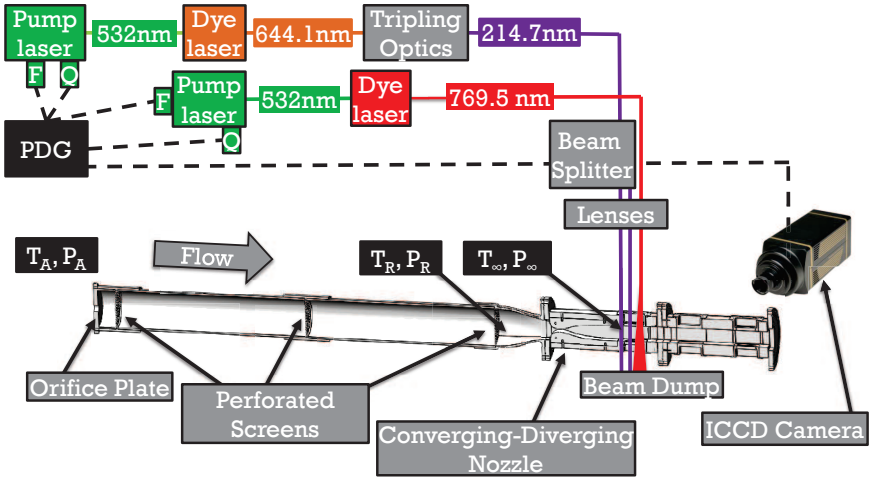

Figure 5: Schematic of KTV-2D experimental setup.

IV. 2-D KTV Data Reduction Algorithm

The goal of the KTV-2D data reduction algorithm is to find the intersections in the grids located in the write and read images. We find the absolute locations of the intersection in the write image relative to the wall using a non-linear regression algorithm. Then the displacements of the intersections in the read images relative to the write images are found using a spatial correlation algorithm. The changes in the x and y coordinates of the intersections, divided by the time then give the u and v components of velocity. The algorithm is different for the write and read images. The locations of the intersections in the write image are found independently, whereas the locations of the intersections in the read images are found by correlating them with their respective windowed write images. The write image is analyzed as follows:

1. Gaussian fitting: Loop through each row in the image and use a Gaussian model to determine the location of the peaks as shown in Fig. 6.

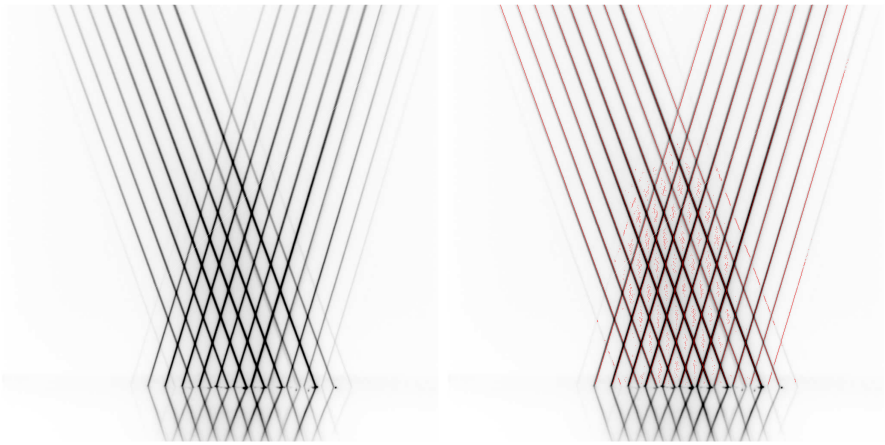

Figure 6: Fluorescence exposures **Left:** Original image. **Right:** Red marks Gaussian fits of write image. False positives picked up by Gaussian fit appear as disconnected red noise in the image.

2. Hough Transform: Apply the Hough transform (similar to procedure Sanchez-Gonzalez et al.[56]) to the Gaussian fits of the write image to locate the lines. Once the equations of the lines are known, their intersections are computed and around each intersection a square window is drawn. These windows are called the source windows. This is shown in Fig. 7.

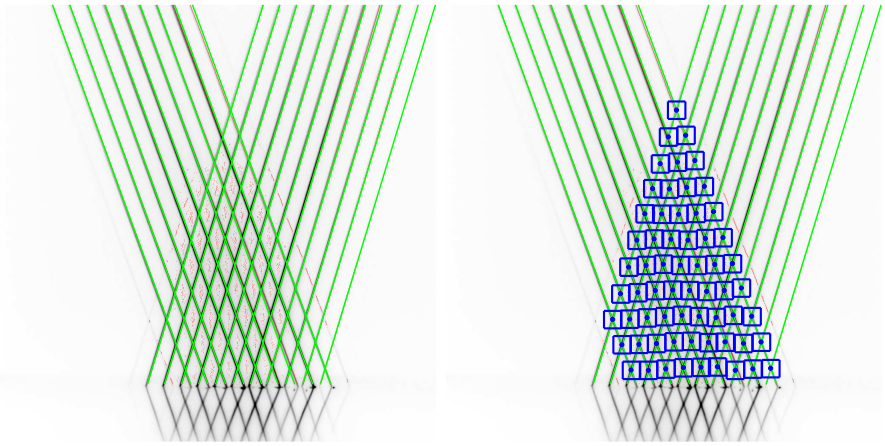

Figure 7: **Left:** Hough transform applied to write image. **Right:** Intersections and source windows.

3. Non-linear regression of intersecting Gaussian lines: The steps above provide a rough estimate of the intersection locations. To get a more accurate result, a model using non-linear regression of intersecting Gaussian lines is applied to the part of the write image inside each source window. This approach is adopted from Ramsey and Pitz.[57] The function, $F = F(x, y, a_1, a_2, c, \theta_1, \theta_2, x_c, y_c) = F(x, y, G)$ is defined as

$$F(x, y, G) = a_1 \exp\left(-\frac{x - b_1}{c}\right)^2 + a_2 \exp\left(-\frac{x - b_2}{c}\right)^2, \tag{1}$$

with G as the vector of fitted parameters. The pixel intensity peaks are given by a_1 and a_2, c is the width of the peak, and to form the lines, $b_1 = \frac{y - y_c}{\tan\theta_1} + x_c$ and $b_2 = \frac{y - y_c}{\tan\theta_2} + x_c$. The angles of the intersecting lines are θ_1 and θ_2, and x_c and y_c are the coordinates of the intersection point. The function F is used to minimize the quantity E against the image intensity in the source window, $I = I(x, y)$, as

$$E = \min_G \sum_{x,y} [F(x, y, G) - I(x, y)]^2. \tag{2}$$

We assume that the optimum values of x_c and y_c give the locations of the intersections in the write image. Fig. 8 shows the source windows with the two best fit lines and the intersection locations.

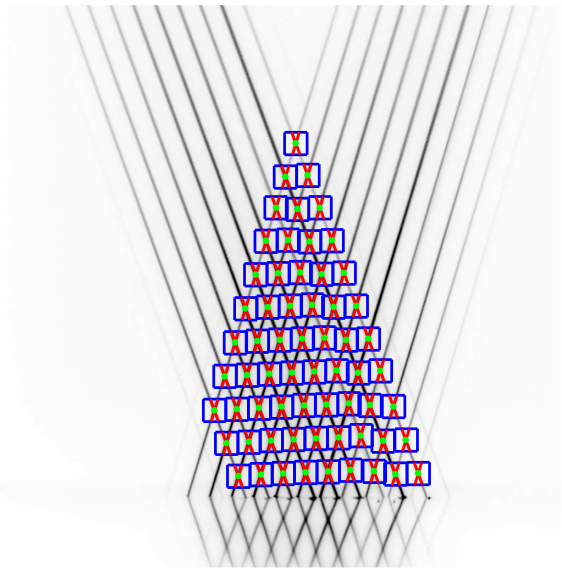

Figure 8: Source windows, best fit lines and intersection points of write image.

To analyze the read images, the method proposed by Gendrich and Koochesfahani[42] was implemented, which involves the use of a correlation function. It is performed in the following steps:

1. Roam Windows: Roam windows are created in the read image for each source window. These roam windows are centered around their corresponding write windows and their dimensions are large enough to contain the displaced intersection point. Fig. 9 shows one write and roam window pair.

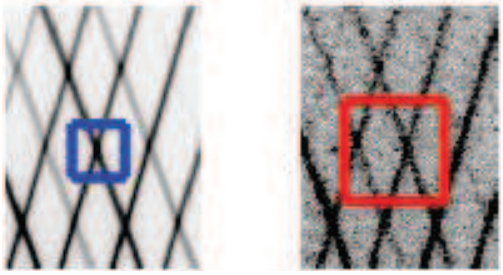

Figure 9: **Left:** Write image with source window. **Right:** Read image with corresponding roam window

2. Spatial Correlation: The spatial correlation function proposed by Gendrich and Koochesfahani[42] is applied to each source/roam window pair in the write image and read image as

$$K(p,q) = -\frac{\overline{I_1 I_2} - \overline{I_1}\,\overline{I_2}}{\sigma_1 \sigma_2}. \tag{3}$$

where $\overline{I_1 I_2}$,$\overline{I_1}$, $\overline{I_2}$, σ_1 and σ_2 are given by,

$$\overline{I_1 I_2} = \frac{\sum_{i,k}\sum_{j,l} I_1(i,j) I_2(k,l)}{MN}. \tag{4}$$

$$\overline{I_1} = \frac{\sum_i \sum_j I_1(i,j)}{MN}. \tag{5}$$

$$\overline{I_2} = \frac{\sum_k \sum_l I_2(k,l)}{MN}. \tag{6}$$

$$\sigma_1 = \sqrt{\frac{\sum_i \sum_j (I_1(i,j) - \overline{I_1})^2}{MN}} \tag{7}$$

$$\sigma_2 = \sqrt{\frac{\sum_k \sum_l (I_2(k,l) - \overline{I_2})^2}{MN}} \tag{8}$$

Here M and N are the dimensions of the source window (in this case equal, since square windows are used), $i = [1, ...M]$, $j = [1, ...N]$,$k = [1 + pmax + p, ...M + pmax + p]$ and $k = [1 + qmax + q, ...N + qmax + q]$. $pmax$ and $qmax$ represent half of the width and height of the roam window respectively. p takes on values from $-pmax$ to $pmax$ and similarly q takes on values from $-qmax$ to $qmax$. $I_1(i,j)$ is the intensity value of the pixel at indices i and j in the source window and similarly $I_2(k,l)$ represents the intensity value of the pixel located at indices k and l in the roam window.

3. Polynomial Fit: The location of the minimum in K determines the location of the intersection in the read image relative to the intersection in the write image, accurate to a pixel. To get sub-pixel accuracy a 5th order 2D polynomial is fitted to the correlation field; however, the entire field is not used, instead a 9x9 pixel region centered around the minimum is used. The location of the minimum value of this polynomial fit then determines the displacement of the intersection relative to its location in the write image. The correlation field and polynomial fit for a roam window are shown in Fig. 10. This algorithm takes roughly 90 minutes to reduce 600 images on a computer with 4 cores running in parallel.

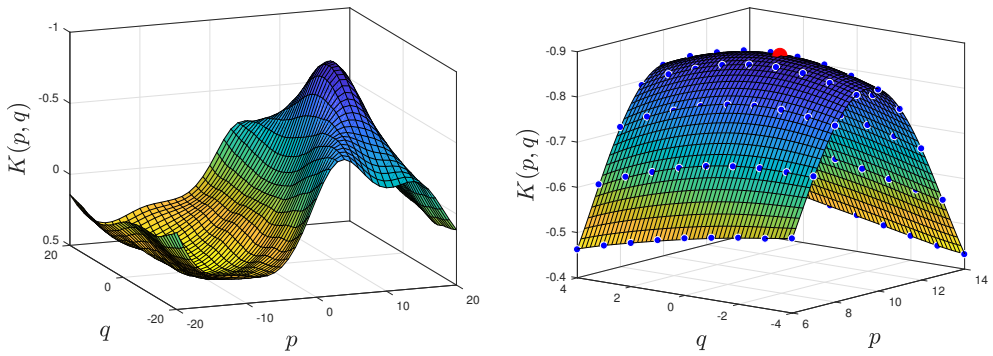

Figure 10: **Left:** Correlation field $K(p, q)$. **Right:** Polynomial fit to correlation field and location of minimum (in red).

V. KTV-2D Boundary Layer Results

Here, we present data from the boundary-layer experiments. It was noted during the data reduction stage that the values calculated for the wall-normal velocity, v, were biased high. This bias was present in all the data taken and the average bias was 57 m/s ($\approx$ 1 pixel). Because we know that in the boundary layer v is approximately zero, this bias was removed by subtracting 57 m/s from all the v values in the data.

Because the same bias appeared in all data sets, we feel confident that it is most likely a systemic issue. We believe that the test section moves slightly on wind tunnel start up, and therefore it can be removed without loss of accuracy, at least in this preliminary work. The write images in the future should be taken with the tunnel on, or a write/read pair should be taken for each exposure. This does not effect the streamwise-component of velocity because the slight test section movement is vertical; no spurious results have been evident in the KTV-1D streamwise-velocity measurements done in the M3CT to date.

Fig. 11 shows the non-dimensionalized mean velocity profiles for the boundary layer, compared to the pitot derived velocity profile and the computational results from the Virginia Tech (VT) Compressible Turbulent Boundary Layer applet.[58]

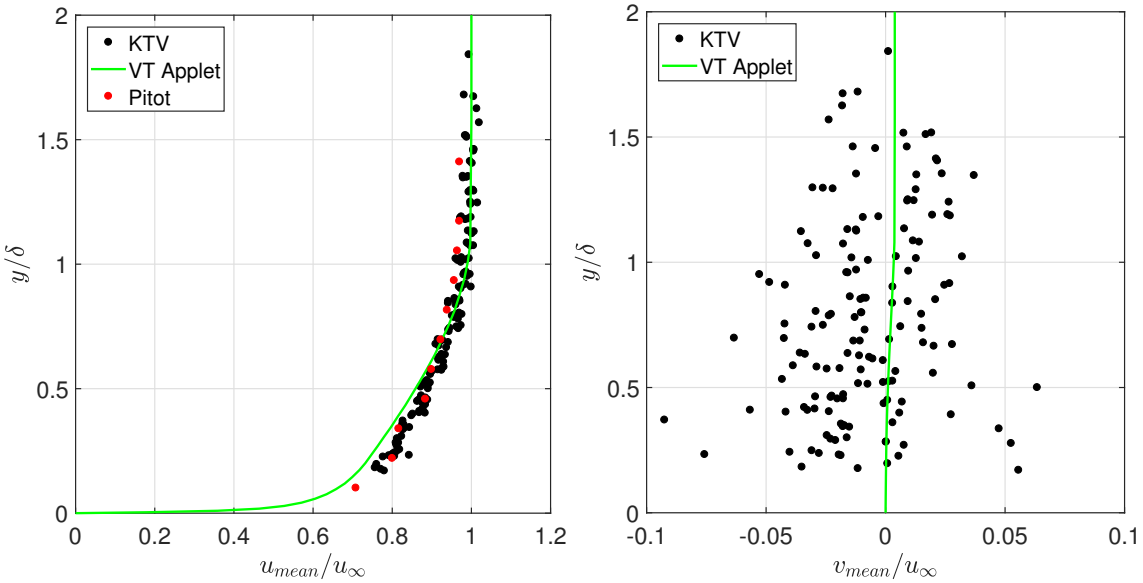

Figure 11: **Left:** Non-dimensional u_{mean} profile. **Right:** Non-dimensional v_{mean} profile.

Fig. 11 shows that u_{mean} agrees well with both the Pitot and the applet velocity profiles. However, v_{mean}

is significantly more noisy. This is because the displacement of each intersection in the y direction is less than a pixel, which is too small to be accurately detected by the data reduction technique, given the noise in the image. Comparatively the displacement in the x direction is on the order of 10 pixels, and is measured more accurately. The u_{mean} data is compared to the logarithmic law, $U^+ = 1/0.41ln(y^+) + 5.2$ in Fig. 12 by applying the Van Driest I transformation with $y^+ = \rho_w \mu_\tau y/\mu_w$ and $U^+ = U/\mu_\tau$. The Van Driest transformation is written as,[59,60]

$$U^+_{VD} = \left[sin^{-1}\left(\frac{R(U^+ + H)}{\sqrt{1 + R^2H^2}}\right) - sin^{-1}\left(\frac{RH}{\sqrt{1 + R^2H^2}}\right)\right]/R \tag{9}$$

with $R = M_\tau\sqrt{(\gamma - 1)Pr_t/2}$, $H = B_q/((\gamma{-}1)M^2_\tau)$, $M_\tau = u_\tau/c_w$ and $B_q = c_f\rho_e U_e(T_w{-}T_r)/(2Pr_e\rho_w u_\tau T_w)$[61](assuming Reynolds analogy holds).

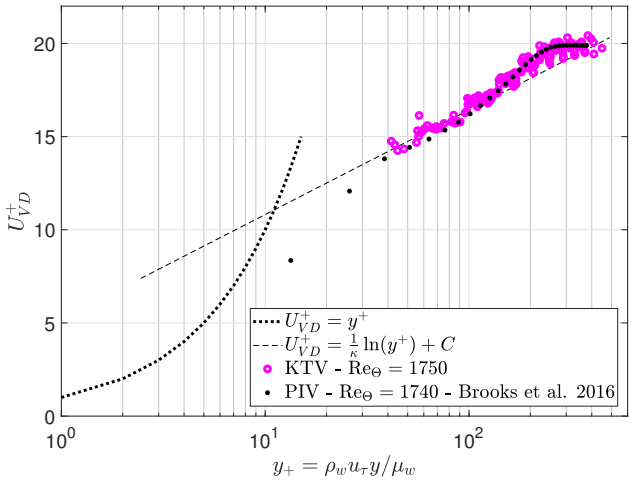

Figure 12: Van Driest scaling of u_{mean}.

The data agrees well with the logarithmic law and the results from Brooks et al.[62] Fig. 13 shows the RMS values of the fluctuating velocity components. Again, the data for u'_{rms} is significantly less noisy than the data for v'_{rms} and shows a clear trend. The v'_{rms} appears to be of the same order as u'_{rms}, which is likely because of the insensitivity to small displacements of the reduction algorithm. When the Morkovin scaling is applied to the fluctuating velocities, u'_{rms} agrees well with results from literature, however v'_{rms} is still uncharacteristically large.

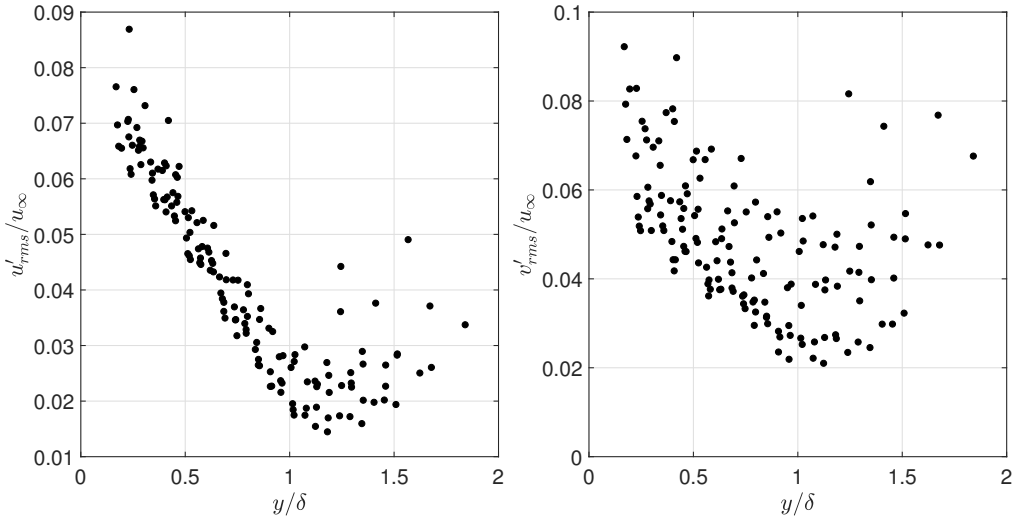

Figure 13: **Left:** Non-dimensional u'_{rms} profile. **Right:** Non-dimensional v'_{rms} profile.

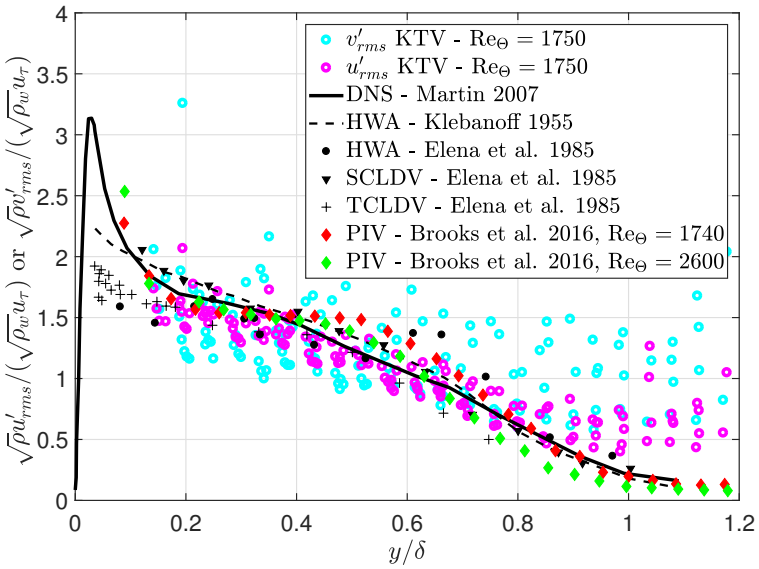

Figure 14: Morkovin scaled fluctuating velocities.

VI. KTV-2D 24 Degree Wedge Results

Here, the results for the flow over the wedge are shown. As in the boundary layer case, the same positive bias was detected in the v component of the velocity and it was removed. Fig. 15 shows the mean velocity vectors with respect to the normalized coordinates. The wedge tip is located at the origin and the wedge is shown in red. The mean shock position (as measured by schlieren) is shown in blue. The data shows the turning angle is between 12 and 15 degrees for the various points near the shock between the shock and the wedge. The value predicted by inviscid theory for the measured local shock angle of 32 degrees is 12.7 degrees. Hence, there is good agreement between the data and the predicted value. The data for v agrees better with expected results for the wedge because the wall-normal displacement after the shock of the intersections is ≈ 2 pixels, which is no longer in the noise.

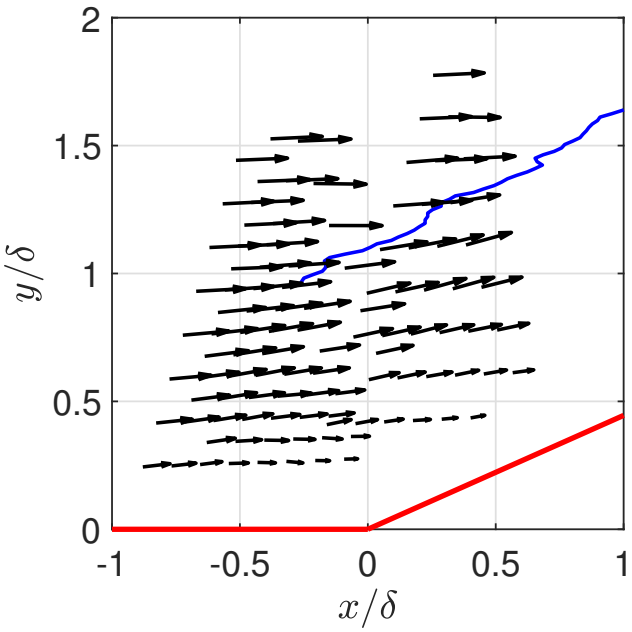

Figure 15: Mean velocity vectors. Wall and wedge marked in red. Mean shock position in blue.

Fig. 16 and 17 show contour plots of the normalized turbulent kinetic energy. These results agree with previous KTV work in the flow over a wedge.[50] The value and location of the maximum normalized turbulent kinetic energy in Fig. 17(left) roughly agree with those reported by Helm et al.,[63] which was however at different conditions ($\mathrm{Re}_\Theta = 2900$). More data closer to the wall would be highly desirable.

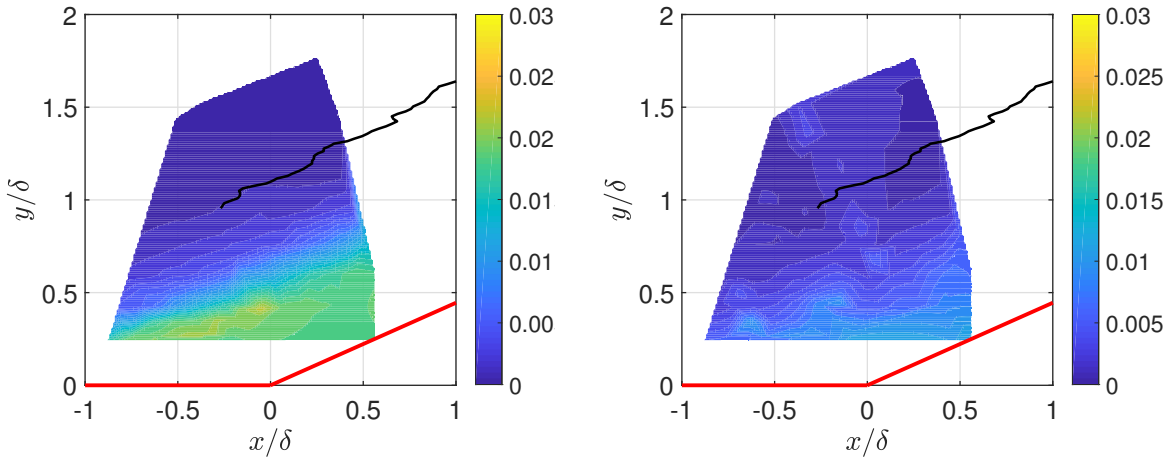

Figure 16: Turbulent kinetic energy contours. Wall and wedge in red, mean shock position in black. **Left:** Turbulent kinetic energy $\frac{u'^2_{rms}}{2u^2_\infty}$. **Right:** Turbulent kinetic energy $\frac{v'^2_{rms}}{2u^2_\infty}$.

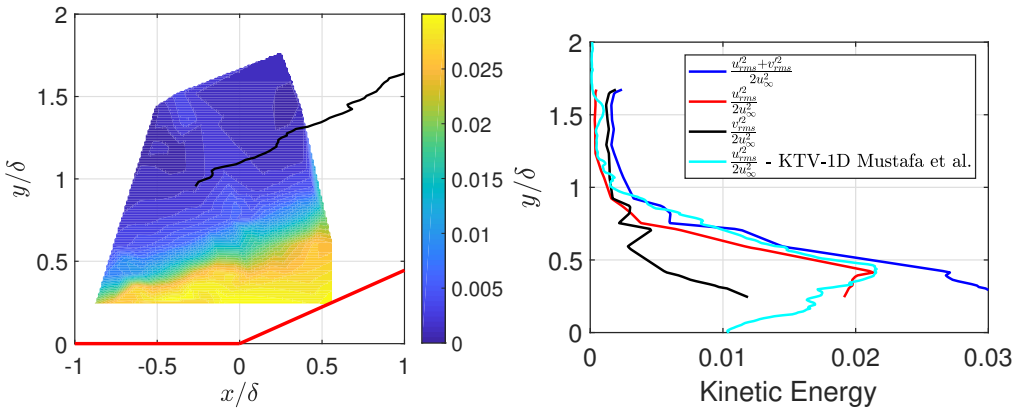

Figure 17: **Left:** Turbulent kinetic energy contour $\frac{u'^2_{rms}+v'^2_{rms}}{2u^2_\infty}$. Wall and wedge in red, mean shock position in black. **Right:** Turbulent kinetic energy at $x = 0$ (wedge tip).

VII. Conclusion

KTV-2D was performed for the first time in a turbulent boundary layer and the flow over a 24 degree wedge. The data was reduced via a correlation algorithm. There was a consistent bias in the v velocity in all data sets, and therefore was determined to be an issue with the procedure (not the KTV technique) and was removed. The relative error for u are comparatively better than results for v because of the relatively small vertical displacements. Furthermore, we believe that the intersection angle of the laser grid, which is ≈ 140 degrees, could be reduced for more accurate measurements of v. An angle closer to 90 will give better results because it will make it easier to locate the intersection. The data for the wedge agrees well with inviscid theory and provides confidence in the goal of utilizing KTV to measure turbulence amplifications across shock waves.

Acknowledgments

The M3CT facilities were supplied by the Arnold Engineering Development Complex (AEDC). The Air Force SFFP supported Mustafa and Parziale with a stipend for this work. Mustafa and Parziale were supported by AFOSR Young Investigator Program Grant FA9550-16-1-0262 and equipment for this work was supported by AFOSR DURIP Grant FA9550-15-1-0325; Ivett Leyva of AFOSR is the Program Manager for both grants. We acknowledge the machine work done by Milan Simonovic and Marshall Reid of Stevens Institute of Technology. We also would like to thank Jonathan Brooks of University of Maryland for assistance with operating the wind tunnel and the Pitot measurements. We would like to acknowledge the encouragement of John Laffery and Dan Marren of AEDC White Oak.

References

[1]Clemens, N. T. and Narayanaswamy, V., "Low-Frequency Unsteadiness of Shock Wave/Turbulent Boundary Layer Interactions," *Annual Review of Fluid Mechanics*, Vol. 46, 2014, pp. 469–492. doi: 10.1146/annurev-fluid-010313-141346.

[2]Andreopoulos, Y., Agui, J. H., and Briassulis, G., "Shock Wave-Turbulence Interactions," *Annual Review of Fluid Mechanics*, Vol. 32, No. 1, 2000, pp. 309–345. doi: 10.1146/annurev.fluid.32.1.309.

[3]Tropea, C., Yarin, A. L., and Foss, J. F., *Springer Handbook of Experimental Fluid Mechanics*, Springer, 2007.

[4]Loth, E., "Compressibility and Rarefaction Effects on Drag of a Spherical Particle," *AIAA Journal*, Vol. 46, No. 9, 2008, pp. 2219–2228. doi: 10.2514/1.28943.

[5]Ragni, D., Schrijer, F.and van Oudheusden, B. W., and Scarano, F., "Particle tracer response across shocks measured by PIV," *Experiments in Fluids*, Vol. 50, No. 1, Jan 2011, pp. 53–64. doi: 10.1007/s00348-010-0892-2.

[6]Elsinga, G. E. and Orlicz, G. C., "Particle imaging through planar shock waves and associated velocimetry errors," *Experiments in Fluids*, Vol. 56, No. 6, Jun 2015, pp. 129. doi: 10.1007/s00348-015-2004-9.

[7]Mitchell, D., Honnery, D., and Soria, J., "Particle relaxation and its influence on the particle image velocimetry cross-correlation function," *Experiments in Fluids*, Vol. 51, No. 4, May 2011, pp. 933. doi: 10.1007/s00348-011-1116-0.

[8]Williams, O. J. H., Nguyen, T., Schreyer, A.-M., and Smits, A. J., "Particle response analysis for particle image velocimetry in supersonic flows," *Physics of Fluids*, Vol. 27, No. 7, 2015, pp. 076101. doi: 10.1063/1.4922865.

[9]Lowe, K. T., Byun, G., and Simpson, R. L., "The Effect of Particle Lag on Supersonic Turbulent Boundary Layer Statistics," *Proceedings of AIAA SciTech 2014*, AIAA-2014-0233, National Harbor, Maryland, 2014. doi: 10.2514/6.2014-0233.

[10]Brooks, J. M., Gupta, A. K., Smith, M. S., and Marineau, E. C., "Particle Image Velocimetry Measurements of Mach 3 Turbulent Boundary Layer at Low Reynolds Numbers," *Submitted*.

[11]Koochesfahani, M. M. and Nocera, D. G., "Molecular Tagging Velocimetry," *Springer Handbook of Experimental Fluid Mechanics*, edited by Tropea, C. and Yarin, A. L. and Foss, J. F., Springer, 2007.

[12]Haertig, J., Havermann, M., Rey, C., and George, A., "Particle Image Velocimetry in Mach 3.5 and 4.5 Shock-Tunnel Flows," *AIAA Journal*, Vol. 40, No. 6, 2002, pp. 1056–1060. doi: 10.2514/2.1787.

[13]Hsu, A. G., Srinivasan, R., Bowersox, R. D. W., and North, S. W., "Molecular Tagging Using Vibrationally Excited Nitric Oxide in an Underexpanded Jet Flowfield," *AIAA Journal*, Vol. 47, No. 11, 2009, pp. 2597–2604. doi: 10.2514/1.39998.

[14]Hsu, A. G., Srinivasan, R., Bowersox, R. D. W., and North, S. W., "Two-component molecular tagging velocimetry utilizing NO fluorescence lifetime and NO_2 photodissociation techniques in an underexpanded jet flowfield," *Applied Optics*, Vol. 48, No. 22, 2009, pp. 4414–4423. doi: 10.1364/AO.48.004414.

[15]Sánchez-González, R., Srinivasan, R., Bowersox, R. D. W., and North, S. W., "Simultaneous velocity and temperature measurements in gaseous flow fields using the VENOM technique," *Optics Letters*, Vol. 36, No. 2, 2011, pp. 196–198. doi: 10.1364/OL.36.000196.

[16]Sánchez-González, R., Bowersox, R. D. W., and North, S. W., "Simultaneous velocity and temperature measurements in gaseous flowfields using the vibrationally excited nitric oxide monitoring technique: a comprehensive study," *Applied Optics*, Vol. 51, No. 9, 2012, pp. 1216–1228. doi: 10.1364/AO.51.001216.

[17]Sánchez-González, R., Bowersox, R. D. W., and North, S. W., "Vibrationally excited NO tagging by NO($A^2\Sigma^+$) fluorescence and quenching for simultaneous velocimetry and thermometry in gaseous flows," *Optics Letters*, Vol. 39, No. 9, 2014, pp. 2771–2774. doi: 10.1364/OL.39.002771.

[18]Dam, N., Klein-Douwel, R. J. H., Sijtsema, N. M., and ter Meulen, J. J., "Nitric oxide flow tagging in unseeded air," *Optics Letters*, Vol. 26, No. 1, 2001, pp. 36–38. doi: 10.1364/OL.26.000036.

[19]Sijtsema, N. M., Dam, N. J., Klein-Douwel, R. J. H., and ter Meulen, J. J., "Air Photolysis and Recombination Tracking: A New Molecular Tagging Velocimetry Scheme," *AIAA Journal*, Vol. 40, No. 6, 2002, pp. 1061–1064. doi: 10.2514/2.1788.

[20]Van der Laan, W. P. N., Tolboom, R. A. L., Dam, N. J., and ter Meulen, J. J., "Molecular tagging velocimetry in the wake of an object in supersonic flow," *Experiments in Fluids*, Vol. 34, No. 4, 2003, pp. 531–534. doi: 10.1007/s00348-003-0593-1.

[21]Miles, R., Cohen, C., Connors, J., Howard, P., Huang, S., Markovitz, E., and Russell, G., "Velocity measurements by vibrational tagging and fluorescent probing of oxygen," *Optics Letters*, Vol. 12, No. 11, 1987, pp. 861–863. doi: 10.1364/OL.12.000861.

[22]Miles, R., Connors, J., Markovitz, E., Howard, P., and Roth, G., "Instantaneous profiles and turbulence statistics of supersonic free shear layers by Raman excitation plus laser-induced electronic fluorescence (RELIEF) velocity tagging of oxygen," *Experiments in Fluids*, Vol. 8, No. 1-2, 1989, pp. 17–24. doi: 10.1007/BF00203060.

[23]Miles, R. B., Zhou, D., Zhang, B., and Lempert, W. R., "Fundamental Turbulence Measurements by RELIEF Flow Tagging," *AIAA Journal*, Vol. 31, No. 3, 1993, pp. 447–452. doi: 10.2514/3.11350.

[24]Miles, R. B. and Lempert, W. R., "Quantitative Flow Visualization in Unseeded Flows," *Annual Review of Fluid Mechanics*, Vol. 29, No. 1, 1997, pp. 285–326. doi: 10.1146/annurev.fluid.29.1.285.

[25]Miles, R. B., Grinstead, J., Kohl, R. H., and Diskin, G., "The RELIEF flow tagging technique and its application in engine testing facilities and for helium-air mixing studies," *Measurement Science and Technology*, Vol. 11, No. 9, 2000, pp. 1272–1281. doi: 10.1088/0957-0233/11/9/304.

[26]Michael, J. B., Edwards, M. R., Dogariu, A., and Miles, R. B., "Femtosecond laser electronic excitation tagging for quantitative velocity imaging in air," *Applied Optics*, Vol. 50, No. 26, 2011, pp. 5158–5162. doi: 10.1364/AO.50.005158.

[27]Edwards, M. R., Dogariu, A., and Miles, R. B., "Simultaneous Temperature and Velocity Measurements in Air with Femtosecond Laser Tagging," *AIAA Journal*, Vol. 53, No. 8, 2015, pp. 2280–2288. doi: 10.2514/1.J053685.

[28]Jiang, N., Halls, B. R., Stauffer, H. U., Danehy, P. M., Gord, J. R., and Roy, S., "Selective two-photon absorptive resonance femtosecond-laser electronic-excitation tagging velocimetry," *Optics Letters*, Vol. 41, No. 10, 2016, pp. 2225–2228. doi: 10.1364/OL.41.002225.

[29]Jiang, N., Mance, J. G., Slipchenko, M. N., Felver, J. J., Stauffer, H. U., Yi, T., Danehy, P. M., and Roy, S., "Seedless velocimetry at 100 kHz with picosecond-laser electronic-excitation tagging," *Optics Letters*, Vol. 42, No. 2, 2017, pp. 239–242. doi: 10.1364/OL.42.000239.

[30]Mills, J. L., *Investigation of Multi-Photon Excitation in Argon with Applications in Hypersonic Flow Diagnostics*, Ph.D. thesis, Old Dominion University, 2016.

[31]McDaniel, J. C., Hiller, B., and Hanson, R. K., "Simultaneous multiple-point velocity measurements using laser-induced iodine fluorescence," *Optics Letters*, Vol. 8, No. 1, 1983, pp. 51–53. doi: 10.1364/OL.8.000051.

[32]Balla, R. J., "Iodine Tagging Velocimetry in a Mach 10 Wake," *AIAA Journal*, Vol. 51, No. 7, 2013, pp. 1–3. doi: 10.2514/1.J052416.

[33]Barker, P., Bishop, A., and Rubinsztein-Dunlop, H., "Supersonic velocimetry in a shock tube using laser enhanced ionisation and planar laser induced fluorescence," *Applied Physics B*, Vol. 64, No. 3, 1997, pp. 369–376. doi: 10.1007/s003400050186.

[34]Lempert, W. R., Jiang, N., Sethuram, S., and Samimy, M., "Molecular Tagging Velocimetry Measurements in Supersonic Microjets," *AIAA Journal*, Vol. 40, No. 6, 2002, pp. 1065–1070. doi: 10.2514/2.1789.

[35]Lempert, W. R., Boehm, M., Jiang, N., Gimelshein, S., and Levin, D., "Comparison of molecular tagging velocimetry data and direct simulation Monte Carlo simulations in supersonic micro jet flows," *Experiments in Fluids*, Vol. 34, No. 3, 2003, pp. 403–411. doi: 10.1007/s00348-002-0576-7.

[36]Handa, T., Mii, K., Sakurai, T., Imamura, K., Mizuta, S., and Ando, Y., "Study on supersonic rectangular microjets using molecular tagging velocimetry," *Experiments in Fluids*, Vol. 55, No. 5, 2014, pp. 1–9. doi: 10.1007/s00348-014-1725-5.

[37]Zhang, S., Yu, X., Yan, H., Huang, H., and Liu, H., "Molecular tagging velocimetry of NH fluorescence in a high-enthalpy rarefied gas flow," *Applied Physics B*, Vol. 123, No. 4, 2017, pp. 122. doi: 10.1007/s00340-017-6703-1.

[38]Boedeker, L. R., "Velocity measurement by H_2O photolysis and laser-induced fluorescence of OH," *Optics Letters*, Vol. 14, No. 10, 1989, pp. 473–475. doi: 10.1364/OL.14.000473.

[39]Wehrmeyer, J. A., Ribarov, L. A., Oguss, D. A., and Pitz, R. W., "Flame Flow Tagging Velocimetry with 193-nm H_2O Photodissociation," *Applied Optics*, Vol. 38, No. 33, 1999, pp. 6912–6917. doi: 10.1364/AO.38.006912.

[40]Pitz, R. W., Lahr, M. D., Douglas, Z. W., Wehrmeyer, J. A., Hu, S., Carter, C. D., Hsu, K.-Y., Lum, C., and Koochesfahani, M. M., "Hydroxyl tagging velocimetry in a supersonic flow over a cavity," *Applied Optics*, Vol. 44, No. 31, 2005, pp. 6692–6700. doi: 10.1364/AO.44.006692.

[41]Hiller, B., Booman, R. A., Hassa, C., and Hanson, R. K., "Velocity visualization in gas flows using laser-induced phosphorescence of biacetyl," *Review of Scientific Instruments*, Vol. 55, No. 12, 1984, pp. 1964–1967. doi: 10.1063/1.1137687.

[42]Gendrich, C. P. and Koochesfahani, M. M., "A spatial correlation technique for estimating velocity fields using molecular tagging velocimetry (MTV)," *Experiments in Fluids*, Vol. 22, No. 1, 1996, pp. 67–77. doi: 10.1007/BF01893307.

[43]Gendrich, C. P., Koochesfahani, M. M., and Nocera, D. G., "Molecular tagging velocimetry and other novel applications of a new phosphorescent supramolecule," *Experiments in Fluids*, Vol. 23, No. 5, 1997, pp. 361–372. doi: 10.1007/s003480050123.

[44]Stier, B. and Koochesfahani, M. M., "Molecular tagging velocimetry (MTV) measurements in gas phase flows," *Experiments in Fluids*, Vol. 26, No. 4, 1999, pp. 297–304. doi: 10.1007/s003480050292.

[45]Ribarov, L. A., Wehrmeyer, J. A., Batliwala, F., Pitz, R. W., and DeBarber, P. A., "Ozone Tagging Velocimetry Using Narrowband Excimer Lasers," *AIAA Journal*, Vol. 37, No. 6, 1999, pp. 708–714. doi: 10.2514/2.799.

[46]Parziale, N. J., Smith, M. S., and Marineau, E. C., "Krypton Tagging Velocimetry for Use in High-Speed Ground-Test Facilities," *Proceedings of AIAA SciTech 2015*, AIAA-2015-1484, Kissimmee, Florida, 2015. doi: 10.2514/6.2015-1484.

[47]Parziale, N. J., Smith, M. S., and Marineau, E. C., "Krypton tagging velocimetry of an underexpanded jet," *Applied Optics*, Vol. 54, No. 16, 2015, pp. 5094–5101. doi: 10.1364/AO.54.005094.

[48]Zahradka, D., Parziale, N. J., Smith, M. S., and Marineau, E. C., "Krypton Tagging Velocimetry (KTV) in Supersonic Turbulent Boundary Layers," *Proceedings of AIAA SciTech 2016*, AIAA-2016-1587, San Diego, California, 2016. doi: 10.2514/6.2016-1587.

[49]Zahradka, D., Parziale, N. J., Smith, M. S., and Marineau, E. C., "Krypton tagging velocimetry in a turbulent Mach 2.7 boundary layer," *Experiments in Fluids*, Vol. 57, No. 62, 2016. doi: 10.1007/s00348-016-2148-2.

[50]Mustafa, M. A., Hunt, M. B., Parziale, N. J., Smith, M. S., and Marineau, E. C., "Krypton Tagging Velocimetry (KTV) Investigation of Shock-Wave/Turbulent Boundary-Layer Interaction," *Proceedings of AIAA SciTech 2017*, AIAA-2017-0025, Grapevine, Texas, 2017. doi: 10.2514/6.2017-0025.

[51]Mustafa, M. A. and Parziale, N. J., "Krypton Tagging Velocimetry in the Stevens Shock Tube," *Proceedings of 33rd AIAA Aerodynamic Measurement Technology and Ground Testing Conference 2017*, AIAA 2017-3897, Denver, Colorado, 2017. doi: 10.2514/6.2017-3897.

[52]Mustafa, M. A., Parziale, N. J., Smith, M. S., and Marineau, E. C., "Nonintrusive Freestream Velocity Measurement in a Large-Scale Hypersonic Wind Tunnel," *AIAA Journal - Accepted - Online*. doi: 10.2514/1.J056177.

[53]Mills, J. L., Sukenik, C. I., and Balla, R. J., "Hypersonic Wake Diagnostics Using Laser Induced Fluorescence Techniques," *Proceedings of 42nd AIAA Plasmadynamics and Lasers Conference*, AIAA 2011-3459, Honolulu, Hawaii, 2011. doi: 10.2514/6.2011-3459.

[54]Balla, R. J. and Everhart, J. L., "Rayleigh Scattering Density Measurements, Cluster Theory, and Nucleation Calculations at Mach 10," *AIAA Journal*, Vol. 50, No. 3, 2012, pp. 698–707. doi: 10.2514/1.J051334.

[55]Chang, R. S. F., Horiguchi, H., and Setser, D. W., "Radiative lifetimes and twobody collisional deactivation rate constants in argon for Kr($4p^5 5p$) and Kr($4p^5 5p$) states," *The Journal of Chemical Physics*, Vol. 73, No. 2, 1980, pp. 778–790. doi: 10.1063/1.440185.

[56]Sánchez-González, R., McManamen, B., Bowersox, R. D. W., and North, S. W., "A method to analyze molecular tagging velocimetry data using the Hough transform," *Review of Scientific Instruments*, Vol. 86, 2015, pp. 105106. doi: 10.1063/1.4932532.

[57]Ramsey, M. C. and Pitz, R. W., "Template matching for improved accuracy in molecular tagging velocimetry," *Experiments in Fluids*, Vol. 51, No. 3, 2011, pp. 811–819. doi: 10.1007/s00348-011-1098-y.

[58]Devenport, W. J. and Schetz, J. A., "Boundary Layer Codes for Students in Java," *Proceedings of the ASME Fluids Engineering Division Summer Meeting*, No. FEDSM98-5139, ASME, Washington, DC, 1998.

[59]Huang, P. G. and Coleman, G. N., "Van Driest Transformation and Compressible Wall-Bounded Flows," *AIAA Journal*, Vol. 32, No. 10, 1994, pp. 2110–2113. doi: 10.2514/3.12259.

[60]Bradshaw, P., "Compressible Turbulent Shear Layers," *Annual Review of Fluid Mechanics*, Vol. 9, No. 1, 1977, pp. 33–52. doi: 10.1146/annurev.fl.09.010177.000341.

[61]Schlichting, H., *Boundary-Layer Theory*, Springer, 2000.

[62]Brooks, J. M., Gupta, A. K., Smith, M. S., and Marineau, E. C., "PIV Measurements of Mach 2.7 Turbulent Boundary Layer with varying Reynolds Numbers," *Proceedings of 54th Aerospace Sciences Meeting, SciTech*, AIAA-2016-1147, San Diego, California, 2016. doi: 10.2514/6.2016-1147.

[63]Helm, C., Martin, M. P., and Dupont, P., "Characterization of the shear layer in a Mach 3 shock/turbulent boundary layer interaction," *Journal of Physics: Conference Series*, Vol. 506, No. 1, 2014, pp. 012013. doi: 10.1088/1742-6596/506/1/012013.